

This is a copy of the published version, or version of record, available on the publisher's website. This version does not track changes, errata, or withdrawals on the publisher's site.

# A case study of using x-ray Thomson scattering to diagnose the in-flight plasma conditions of DT cryogenic implosions

H. Poole, D. Cao, R. Epstein, I. Golovkin, T. Walton, S. X. Hu, M. Kasim, S. M. Vinko, J. R. Rygg, V. N. Goncharov, G. Gregori, and S. P. Regan

## Published version information

**Citation:** H Poole et al. A case study of using x-ray Thomson scattering to diagnose the in-flight plasma conditions of DT cryogenic implosions. *Phys Plasmas* 29, no. 7 (2022): 072703

**DOI:** [10.1063/5.0072790](https://doi.org/10.1063/5.0072790)

This article may be downloaded for personal use only. Any other use requires prior permission of the author and AIP Publishing. This article appeared as cited above.



This version is made available in accordance with publisher policies. Please cite only the published version using the reference above. This is the citation assigned by the publisher at the time of issuing the APV. Please check the publisher's website for any updates.

This item was retrieved from **ePubs**, the Open Access archive of the Science and Technology Facilities Council, UK. Please contact [epublications@stfc.ac.uk](mailto:epublications@stfc.ac.uk) or go to <http://epubs.stfc.ac.uk/> for further information and policies.

# A case study of using x-ray Thomson scattering to diagnose the in-flight plasma conditions of DT cryogenic implosions

Cite as: Phys. Plasmas **29**, 072703 (2022); <https://doi.org/10.1063/5.0072790>

Submitted: 24 September 2021 • Accepted: 12 June 2022 • Published Online: 05 July 2022

 H. Poole,  D. Cao,  R. Epstein, et al.



View Online



Export Citation



CrossMark

## ARTICLES YOU MAY BE INTERESTED IN

[Role of self-generated magnetic fields in the inertial fusion ignition threshold](#)

Phys. Plasmas **29**, 072701 (2022); <https://doi.org/10.1063/5.0091529>

[Hybrid Zakharov-kinetic simulation of nonlinear stimulated Raman scattering](#)

Phys. Plasmas **29**, 072103 (2022); <https://doi.org/10.1063/5.0090211>

[Progress toward fusion energy breakeven and gain as measured against the Lawson criterion](#)

Phys. Plasmas **29**, 062103 (2022); <https://doi.org/10.1063/5.0083990>



Physics of Plasmas  
Features in Plasma Physics Webinars

Register Today!

# A case study of using x-ray Thomson scattering to diagnose the in-flight plasma conditions of DT cryogenic implosions

Cite as: Phys. Plasmas **29**, 072703 (2022); doi: 10.1063/5.0072790

Submitted: 24 September 2021 · Accepted: 12 June 2022 ·

Published Online: 5 July 2022



View Online



Export Citation



CrossMark

H. Poole,<sup>1,a)</sup> D. Cao,<sup>2</sup> R. Epstein,<sup>2</sup> I. Golovkin,<sup>3</sup> T. Walton,<sup>3</sup> S. X. Hu,<sup>2,4</sup> M. Kasim,<sup>1</sup> S. M. Vinko,<sup>1,5</sup> J. R. Rygg,<sup>2,4</sup> V. N. Goncharov,<sup>2,4</sup> G. Gregori,<sup>1</sup> and S. P. Regan<sup>2,4</sup>

## AFFILIATIONS

<sup>1</sup>Department of Physics, University of Oxford, Oxford OX1 3PU, United Kingdom

<sup>2</sup>Laboratory for Laser Energetics, University of Rochester, Rochester, New York 14623, USA

<sup>3</sup>Prism Computational Sciences, Madison, Wisconsin 53711, USA

<sup>4</sup>Department of Mechanical Engineering, University of Rochester, Rochester, New York 14611, USA

<sup>5</sup>Central Laser Facility, STFC Rutherford Appleton Laboratory, Didcot OX11 0QX, United Kingdom

<sup>a)</sup>Author to whom correspondence should be addressed: [hannah.poole@physics.ox.ac.uk](mailto:hannah.poole@physics.ox.ac.uk)

## ABSTRACT

The design of inertial confinement fusion ignition targets requires radiation-hydrodynamics simulations with accurate models of the fundamental material properties (i.e., equation of state, opacity, and conductivity). Validation of these models is required via experimentation. A feasibility study of using spatially integrated, spectrally resolved, x-ray Thomson scattering measurements to diagnose the temperature, density, and ionization of the compressed DT shell of a cryogenic DT implosion at two-thirds convergence was conducted. Synthetic scattering spectra were generated using 1D implosion simulations from the LILAC code that were post processed with the x-ray scattering model, which is incorporated within SPECT3D. Analysis of two extreme adiabat capsule conditions showed that the plasma conditions for both compressed DT shells could be resolved.

Published under an exclusive license by AIP Publishing. <https://doi.org/10.1063/5.0072790>

## I. INTRODUCTION

The design of inertial confinement fusion (ICF) targets is a challenging task that requires, among others, hydrodynamic simulations with knowledge of the shocked materials' equation of state (EOS) if ignition conditions are to be achieved.<sup>1–5</sup> The theoretical modeling of the extreme matter properties reached during the capsule implosion is difficult due to the need of a quantum mechanical treatment of the degenerate electrons, moderate strongly coupled ions, and many-particle correlations.<sup>6–9</sup> Uncertainty in the EOS of matter under this regime results in unconfirmed calculations for transport properties, ionization balance, and energy and temperature equilibration.<sup>10–14</sup> Therefore, experimental validation is vital for benchmarking and developing reduced models that can be implemented in radiation hydrodynamic codes.

At present, the diagnosis of the physical properties of dense plasmas produced in ICF implosions is limited due to the difficulty in achieving the required accuracy and spatial resolutions<sup>15–18</sup> for different model predictions to be tested. Over the past couple of decades,

there has been a push to develop new diagnostics that may be able to resolve different regions of the imploding capsule. Multi-keV spectrally resolved x-ray Thomson scattering (XRTS) is one of these techniques.<sup>18–20</sup> Presented here is a methodology for resolving the in-flight compressed shell conditions.

The first experimental observation of noncollective, inelastic x-ray scattering from shocked liquid deuterium is discussed in Ref. 17. This demonstrated the capabilities of inferring the electron temperature, ionization, and electron density from the shapes and intensities of the elastic (Rayleigh) and inelastic (Compton) components in the scattering spectra in ICF dense matter. However, the scattering data had no spatial information and the analysis performed did not provide the capability to separate the contribution from different regions.

Spatial temperature and ionization profiles were determined from a near-solid density foam using a collimated x-ray beam in Ref. 21. These data, produced using the imaging x-ray Thomson spectrometer (IXTS) at the Omega laser facility,<sup>22,23</sup> determined the temperature and ionization state of the carbon foam at multiple positions

along the axis of the flow. Good agreement was found between the experiment and theoretical predictions with the exception of the high-temperature, low-density rarefaction region of the blast wave.

Simultaneous collective and non-collective scattering data for dynamically compressed deuterium were collected in Ref. 24 using the 2 keV Si Ly- $\alpha$  line. This focused on compression states of  $\rho/\rho_0 \sim 2.8\text{--}4.05$ . The mass density was determined using the VISAR shock velocity using current EOS data. This allowed for a restriction on the parameter space when determining the ionization from the XRTS data.

To date, experiments have successfully been conducted at the Omega laser facility to determine conditions on spherical CH implosions in Refs. 25 and 26. However, no attempt has yet been made to field an XRTS diagnostic on a laser direct-drive ICF implosion of a layered, cryogenic deuterium-tritium (DT) spherical target. In this report, the feasibility of utilizing spatially integrated XRTS measurements to determine the in-flight conditions of the compressed DT shell will be investigated. This study involved analyzing the x-ray scattering data produced by targets with very different adiabats. The adiabat is defined as the ratio of the plasma pressure to the Fermi-degenerate pressure,<sup>27</sup> and for DT fuel, it is given by<sup>28</sup>

$$\alpha_{DT} \simeq \frac{P_{\text{Shell}} [\text{Mbar}]}{2.2[\rho [\text{g}/\text{cm}^3]]^{5/3}}. \quad (1)$$

Confinement properties of an ICF capsule depend on the areal density of the compressed shell and hot-spot,  $\rho R$ . The areal density is controlled by varying the entropy of the fuel, which is determined by the fuel adiabat. For ignition to occur, a large enough areal density (low adiabat),  $>0.2\text{--}0.5 \text{ g}/\text{cm}^2$ , and hot enough core,  $\sim 5\text{--}12 \text{ keV}$ , are required.<sup>29,30</sup> However, targets imploded on a low adiabat are susceptible to hydrodynamic instabilities<sup>31,32</sup> that drive the rapid growth of nonuniformities. Therefore, an important part of ICF research involves optimization of the adiabat.<sup>33–35</sup> In experiments, however,

direct measurements of the in-flight fuel adiabat and densities are not yet achievable, instead they are inferred from the neutron yield and x-ray self-emission.<sup>36</sup>

For this feasibility paper, the target chosen for the high adiabat design was used in the first phase of the performance optimization campaign (this campaign has since set the record for neutron yield on OMEGA<sup>37</sup>) and is considered a good design reference point for a stable implosion. The lower adiabat target design used was part of a campaign to probe performance right below an observed “stability cliff”<sup>38</sup> that is still considered in modern implosion designs on OMEGA.

This paper presents dual-channel XRTS as a possible diagnostic to retrieve spatial information on the in-flight conditions of an ICF implosion. The analysis is performed by constructing synthetic, spatially integrated, spectra using the collision-radiative code SPECT3D,<sup>39</sup> including the x-ray scattering simulator,<sup>40</sup> which is a post-processor of the 1D radiation hydrodynamic code LILAC.<sup>41</sup>

## II. PROPOSED EXPERIMENTAL SETUP

XRTS is a powerful diagnostic tool for determining the conditions in plasmas where the critical density,  $n_c = \epsilon_0 m_e \omega^2 / e^2$  (where  $m_e$  is the mass of an electron,  $e$  is the electron charge,  $\epsilon_0$  is the electric constant, and  $\omega$  is the frequency of the laser drive), exceeds what can be probed by any optical source. The first consideration for an experimental setup is the power required for the x-ray probe in order to produce a scattering signal that can be observed above background noise. The total number of photons in the free-free scattering feature,  $N_{\text{scatt}}$ , can be estimated as<sup>18</sup>

$$N_{\text{scatt}} = \left( \frac{E_L}{h\nu} \eta_x \right) \left( \frac{\Omega_{\text{plasma}}}{4\pi} \eta_{\text{att}} \right) \left( \frac{n_e \sigma_{\text{Th}} \ell}{(1 + \alpha)^2} \right), \quad (2)$$

where  $E_L$  is the probe laser energy,  $\eta_x$  is the conversion efficiency from the laser energy into the probe x-rays,  $\eta_{\text{att}}$  is the attenuation of the

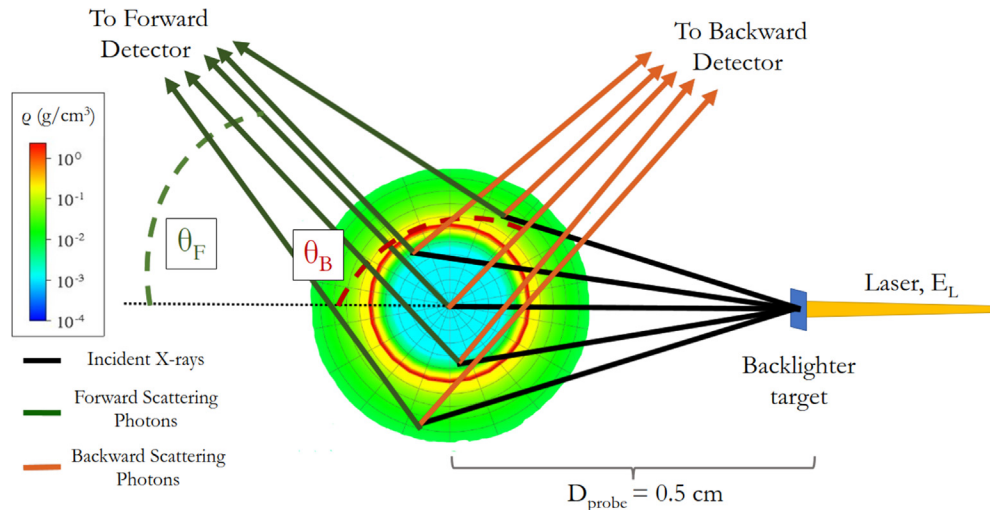


**FIG. 1.** A sketch of the proposed experimental setup, with a laser energy  $E_L$  incident on a backlighter target, producing x-rays with a conversion efficiency of  $\eta_x$ . The scattering x-rays are shown incident on the 3D inferred density profile from Spect3D using the 1D simulation data produced by the LILAC code. Schematic of the scattering events, recorded on the detector by SPECT3D, from different zones throughout the implosion is shown. The scattering geometry is demonstrative and not drawn to scale.

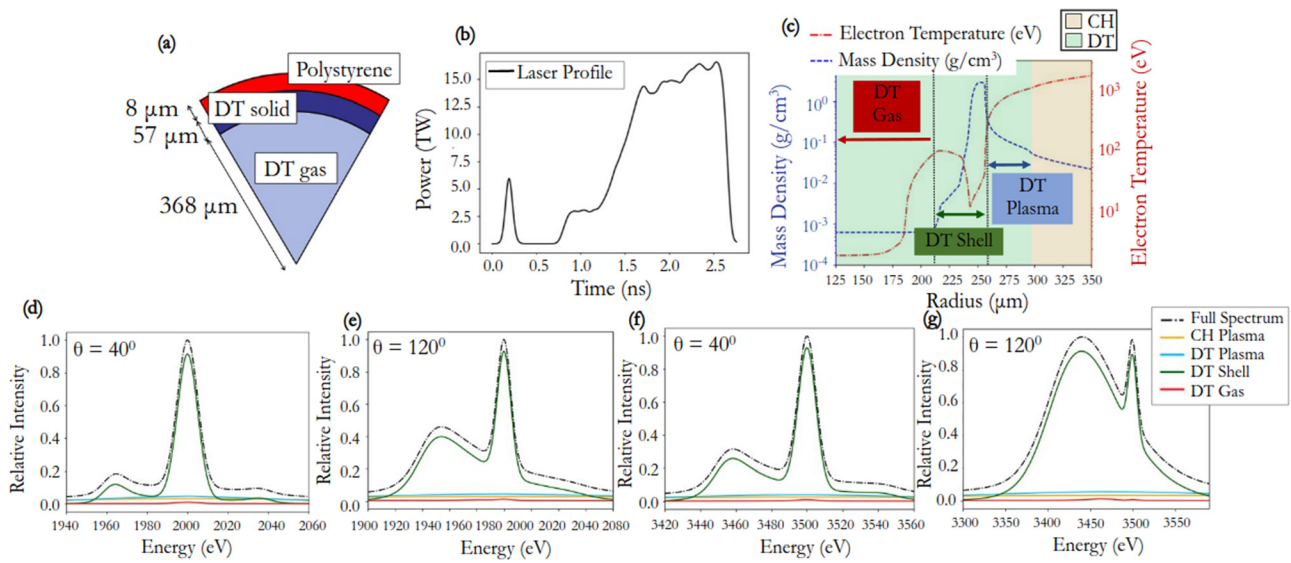


**FIG. 2.** (a) Simulated target design, with an adiabat of 2.8, fired with laser profile shown in (b). (c) Density and electron temperature conditions in the ICF implosion across the shock wave (propagating to the left) at two-thirds compression,  $t = 2215$  ps, as determined by the LILAC code for the target. The scattering contributions from the DT in the unshocked fuel, compressed shell, and coronal plasma have been isolated and compared to the fully integrated spectrum. For a 2 keV probe, the contribution from each region of the plasma to the overall scattering spectrum is shown for both the forward ( $40^\circ$ ) (d) and backward ( $120^\circ$ ) scattering regimes (e). The same breakdown of the plasma has been performed with a 3.5 keV energy probe in (f) and (g).

probe x-rays through the dense plasma,  $\Omega_{\text{plasma}}$  is the solid angles subtended by the plasma,  $n_e$  is the electron density,  $\alpha$  is the scattering parameter,  $\sigma_{\text{Th}}$  is the Thomson scattering cross-section, and  $\ell$  is the path length of the photons through the plasma.

For the plasma conditions investigated here, the scattering fraction,  $n_e \sigma_{\text{Th}} \ell$ , is approximately equal to  $10^{-4}$ , where representative values for the compressed shell have been taken as  $n_e \sim 10^{23} \text{ cm}^{-3}$  and

$\ell = 75 \mu\text{m}$ . This small scattering fraction makes fielding XRTS challenging since the signal can easily be swamped by significant self-emission from the plasma.

A key benefit of fielding XRTS as a plasma diagnostic is that XRTS can be split into two scattering regimes, the collective and the noncollective, as determined by the scattering parameter,

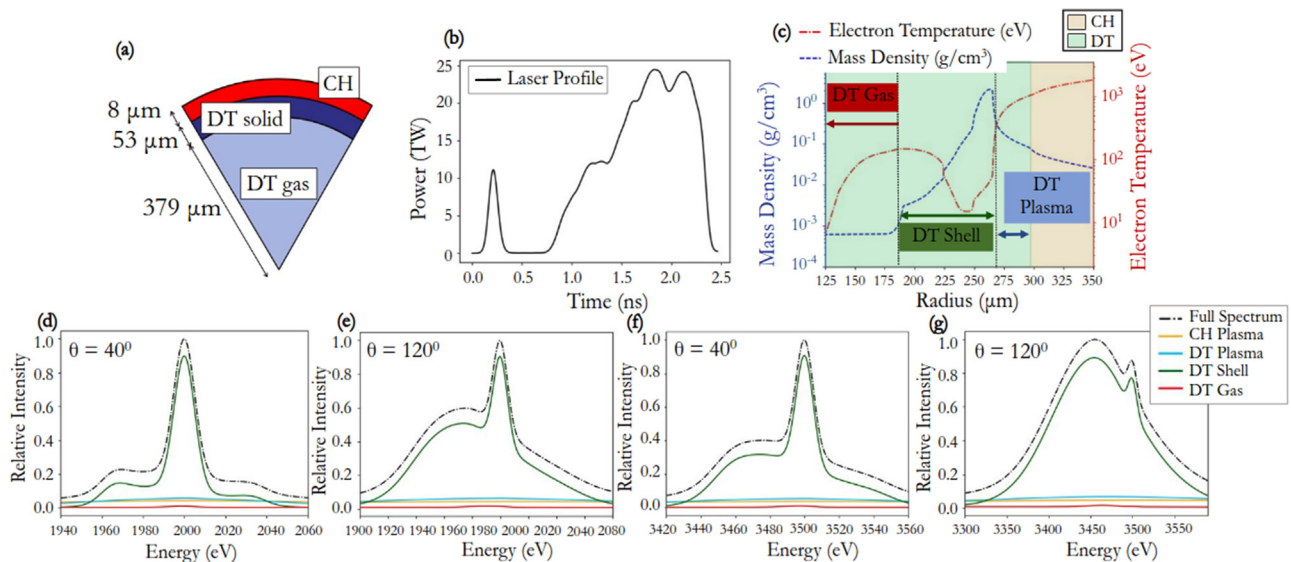


**FIG. 3.** As with Fig. 2 but with an ICF capsule with an adiabat of 8.0 and at  $t = 1901$  ps.



$$\alpha = \frac{1}{k\lambda_s}, \tag{3}$$

where  $k$  is the scattering vector and  $\lambda_s$  is the screening length. In the noncollective regime, the incoming wave “probes” through the screening sphere and the scattering spectrum, therefore, reflect the electron velocity distribution. In contrast, the collective scattering regime reflects the collective motion of the electrons. Designing an experiment where both regimes can be recorded can reduce the error on the inferred plasma parameters.

To model the x-ray emissivity, a 1 kJ laser with a 10 ps pulse length and a source diameter of 50  $\mu\text{m}$  were used to produce a Gaussian x-ray source, with a FWHM of 10 eV, 0.5 cm away from the imploding target, taking an estimate of  $\eta_x = 0.01\%$ .<sup>42</sup> This backlighter distance is possible due to the development of a fast target positioner (FASTPOS) in cryogenic implosion by Stoeckl *et al.*<sup>43</sup> The demonstrative scattering geometry is shown in Fig. 1. With these laser and plasma parameters, using Eq. (2), the total number of scattered photons is  $\sim 3 \times 10^7$ . The forward scattering was collected at  $\theta_F = 40^\circ$  and the backward scattering at  $\theta_B = 120^\circ$ . The details of the two targets chosen for this investigation are shown in Figs. 2 and 3 with adiabats of 2.8 and 8.0, respectively.

Two experimental setups are considered for this paper, one with an x-ray probe energy of 2 keV and the other using a 3.5 keV probe. The scattering regime recorded by each detector in each setup is shown in Fig. 4. These two probe energies were selected to investigate the effect of different laser energies that had on the determined plasma parameters while keeping one detector in the collective and the other in the noncollective regimes. It should be noted that the values for the  $\alpha$  parameter shown in the figure are calculated for the densest region in the compressed DT shell and, therefore, not representative of the scattering from the ICF capsule as a whole. To determine the scattering signals from each region of the implosion, the fully integrated scattering spectra must be determined.

The plasmon frequency shift for the high adiabat target is  $\sim 27$  eV, which increases to  $\sim 30$  eV for the low adiabat target. In order

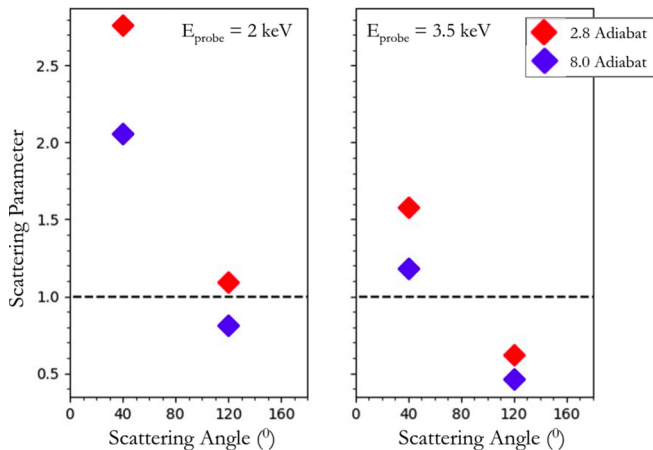


**FIG. 4.** Scattering parameters,  $\alpha$ , as calculated for the densest zone in the compressed DT shell for each adiabat, scattering angle, and probe energy. A dashed line is shown at  $\alpha = 1$ , which is the approximate separation of collective,  $\alpha > 1$ , and noncollective,  $\alpha \leq 1$ , scatterings.

to distinguish this plasmon scattering, a narrow band x-ray probe must be used (FWHM  $< 10$  eV). To achieve this in an experimental setup, the source must be chosen carefully.

Previous experiments have successfully used a crystal imaging system with a Si He $\alpha$  line at  $\sim 1.865$  keV to radiograph OMEGA cryogenic implosions,<sup>44</sup> but the required x-ray fluence may not be enough. Alternatively, Cl K $\alpha$  at  $\sim 2.62$  keV or Cl Ly- $\alpha$  at  $\sim 2.96$  keV could be used.<sup>45</sup>

An important consideration to make before extrapolating this work to an experimental campaign is predicting the level of noise on the scattering signal. In the case of a fusion capsule implosion, there is significant self-emission that will be collected over the time gating of the detector. Representative spectra have been produced for this case study as detailed below.

### III. OBTAINING SIMULATED SPATIALLY INTEGRATED SPECTRA

The cryogenic DT implosion plasma conditions were calculated using the LILAC code. The LILAC code is a 1D spherical Lagrangian, radiation-hydrodynamics code<sup>41</sup> that simulates symmetric, laser direct-drive implosions. It includes laser ray-tracing with an inverse bremsstrahlung model that can also account for cross-beam energy transfer.<sup>46</sup> LILAC also includes a nonlocal thermal transport model that uses a simplified Boltzmann equation with a Krook collision term,<sup>47</sup> multi-group radiation diffusion, and a first-principles equation-of-state (FPEOS) model<sup>48,49</sup> and a opacity (FPOT) model<sup>50</sup> derived from molecular dynamics methods.

In this work, the focus is on the time when the capsule is at two-thirds compression,  $R_{\text{Ablation surface}}/R_{\text{Vapor, initial}} = 2/3$ . The inhomogeneity of the plasma results in different scattering signals from different regions of the plasma. The capability to simulate the fully spatially integrated spectra, accounting for opacity and self-emission of the

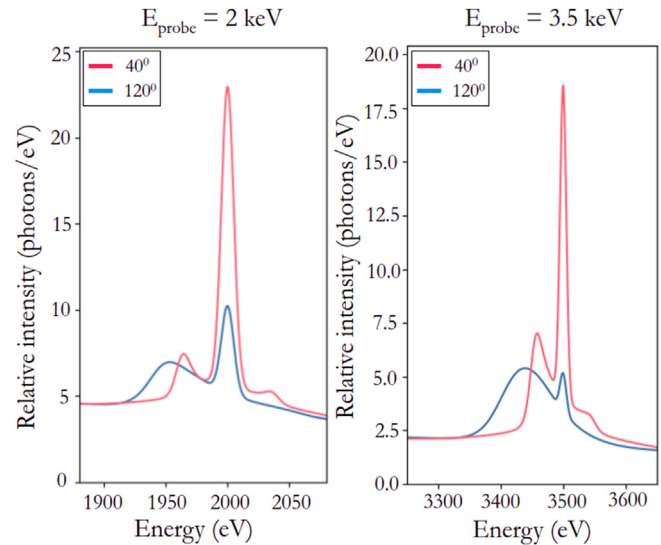


**FIG. 5.** Total relative detected signal per eV, where  $\Gamma_{\text{det}}$  is assumed to be  $10^{-5}$ , integrated over the time of the x-ray laser pulse = 10 ps. The signal is shown for the target with an adiabat of 2.8 with both the 2 keV and 3.5 keV laser photon energies.

plasma, is paramount to determine, for a given scattering geometry, the dominant scattering features. This provides insightful information to design the experiments.

SPECT3D is a spectroscopy code produced by Prism Computational Sciences, which post-processes hydrodynamics code output and simulates high-resolution spectra and images for local thermodynamic equilibrium (LTE) and non-LTE plasmas in 1D, 2D, and 3D geometries.<sup>39</sup> It computes a variety of diagnostic signatures that can be compared with experimental measurements including: time-resolved and time-integrated spectra, space-resolved spectra and streaked spectra, filtered and monochromatic images, and x-ray diode signals. In a SPECT3D simulation, the radiation incident at a detector is computed by solving the radiative transfer equation along a series of lines-of-sight (LOSs) through the plasma grid. At each plasma volume element along a LOS, the frequency-dependent absorption and emissivity of the plasma are calculated. The scattering cross-section is computed using local values of the plasma conditions based on the formalism originally developed in Refs. 51 and 52. Scattered x-ray photons are added to the local source function, allowing SPECT3D to utilize the same algorithms as it uses for plasma self-emission. It is assumed that the radiation from a non-monochromatic, isotropically emitting point-like x-ray source is scattered within each volume

element of the SPECT3D spatial grid. The source is specified by its photon-energy-dependent intensity and location in 3D space. The intensity of the radiation from the source is adjusted for each volume element based on the distance to the source. It includes attenuation due to plasma absorption and the change in the solid angle. The radiation flux at each pixel in the detector plane is calculated by integrating the scattered radiation along each LOS. The scattering angle is computed for each volume element based on the LOS and the line that connects the volume element center and the source.<sup>40</sup>

For this paper, an additional feature was added to the original implementation, which allows for certain plasma cells to be excluded from contributing to the scattered signal. This allows for studying the contribution of particular plasma regions to the total scattered spectrum. Models for computing self-emission and absorption coefficients remain the same in each zone regardless of whether the flag for excluding scattered signal is set or not.

The addition of this feature allows spectra from isolated regions of the plasma to be compared to the fully integrated spectra in Figs. 2 and 3. The overall spectral shape in each detector is dominated by the scattering from the compressed DT shell due to its high density compared to the hot CH plasma. This gives us confidence that an experiment designed to retrieve scattering spectra at this time during the

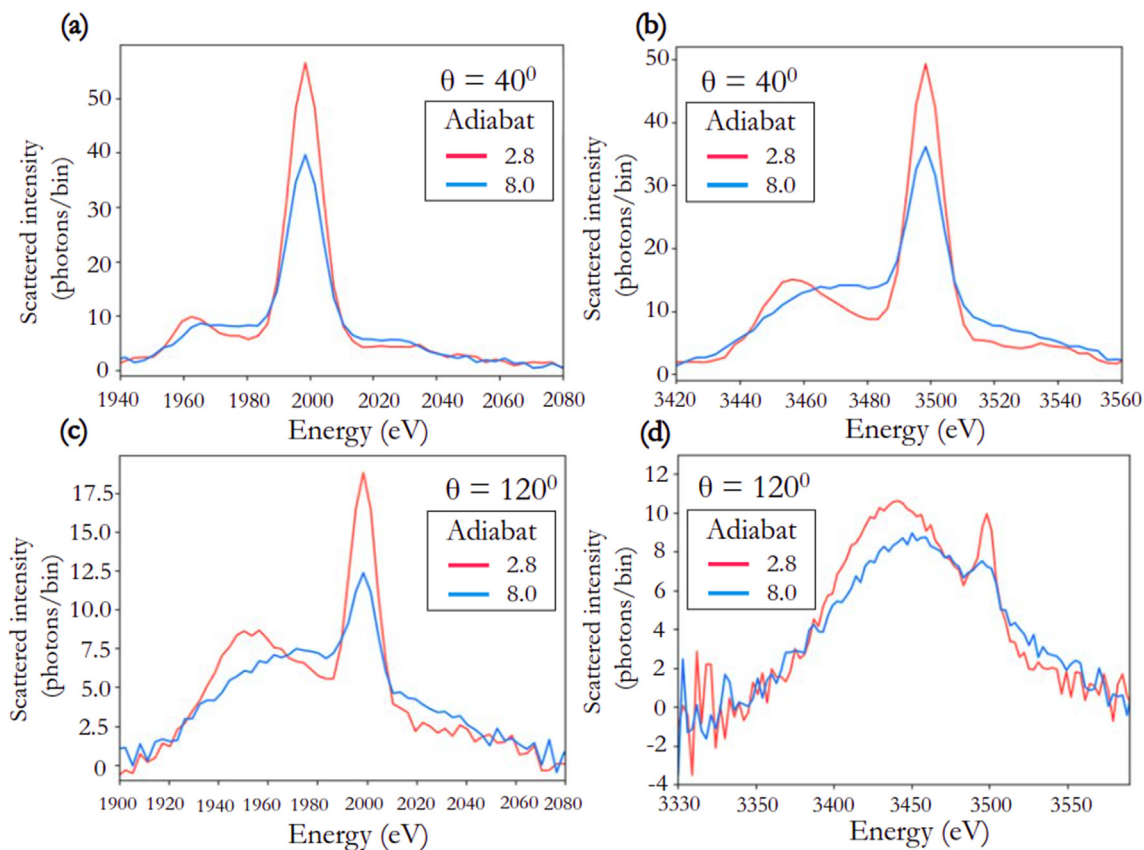


**FIG. 6.** Synthetic experimental x-ray scattering data produced by Spect3D for LILAC simulations with adiabats of 2.8 and 8.0, assuming 3 eV/bin and Poisson statistics to simulate noise. (a) and (b) Forward scattering spectra for a 2 keV probe and a 3.5 keV probe, respectively. (c) and (d) Backward scattering spectra for a 2 keV probe and a 3.5 keV probe, respectively.

implosion will be representative of the conditions in the compressed shell.

The spectra in Fig. 5 demonstrate the relative strength of the scattering signal to the continuum emission over the timescale of the x-ray laser pulse. The number of detected photons in the free-free scattering feature is calculated as<sup>53</sup>

$$N_d = N_{\text{scatt}} \times \left( \frac{\Omega_{\text{det}}}{4\pi} R_{\text{crystal}} \eta_d \right) = N_{\text{scatt}} \times \Gamma_{\text{det}}, \quad (4)$$

where  $\Gamma_{\text{det}}$  is the fraction of detected photons determined by  $\Omega_{\text{det}}$ ,  $R_{\text{crystal}}$ , and  $\eta_d$ , which are the solid angle of the detector, the reflectivity of the crystal, and the detector efficiency, respectively. For this case study, a  $\Gamma_{\text{det}} \sim 10^{-5}$  is assumed, which gives  $N_d \sim 300$  to produce a signal capable of resolving the adiabats. This assumption gives approximately 3 photons/eV contributing to the inelastic feature, as shown in Fig. 5. Taking a spectral resolution of 3 eV/bin gives  $\sim 9$  photons/bin. With currently available spectrometers, such as ZSPEC at the OMEGA laser facility,<sup>54</sup> we can readily achieve  $\Gamma_{\text{det}} \sim 10^{-6}$ . While this would produce a signal that is only marginally measurable, increasing the fraction of detected photons could be realized, for example, with a modified design consisting of a disposable x-ray crystal placed much closer to the imploding capsule or employing new generation of detectors with higher quantum efficiency.

Synthetic experimental noise was added by removing the uniform background signal from the spectra, assuming a logarithmic fit, and using Poisson statistics, which estimates the noise as  $\sim 1/\sqrt{N_i}$ ,

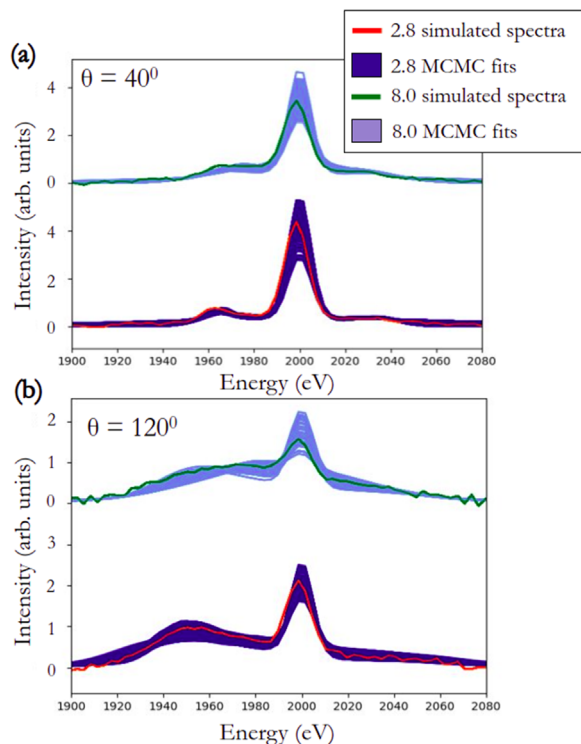


FIG. 7. Accepted MCMC fits using a 2 keV photon energy probe with the (a)  $40^\circ$  and (b)  $120^\circ$  detectors.

where  $N_i$  is the number of photons per spectral resolution element. The resultant spectra are shown in Fig. 6.

Utilizing XRTS to determine the adiabat of an ICF capsule would be a valuable diagnostic development. Figure 6 demonstrates that for experimental conditions with identical scattering setups, the two extreme adiabat conditions considered here produce notably differing scattering spectra. In both the 2 and 3.5 keV case, the plasmon scattering seen in the forward scattering detector can be used to determine the difference in electron density between the two adiabats. The difference between the inelastic scattering features from the two adiabats seen in Fig. 6(c) is a result of only the low adiabat remaining in the collective scattering regime. The high adiabat's inelastic scattering feature has become dominated by Compton scattering. This is evidenced by the broadening of the inelastic peak and the lose of a forward plasmon shift peak. This change in scattering features is evidence of its higher electron temperature and lower density.

#### IV. RESULTS

Before extracting the plasma parameters from the spatially integrated simulated spectra, the inverse problem instability must first be addressed, which implies that the same measured spectra could be fitted equally well by very different plasma parameters.<sup>55</sup> Bayesian inference, using Markov-Chain Monte Carlo (MCMC) to sample the multidimensional space, is a more robust approach to explore the behavior of the complex multiparameter simulations.<sup>56</sup>

An MCMC exploration fit the entire spectra, assuming two weighted uniform plasma regions: one containing DT and the other CH. While it must be acknowledged that the plasma, as demonstrated above, is not uniform, when performing the MCMC analysis, it is impractical to fit multiple plasma regions to the plasma. This is because to implement this, the searched parameter space for each region would need to be restricted to prevent it from overlapping with others. This would ruin the inherently unbiased analysis performed here. Part of this feasibility research involved resolving how and if the resultant parameters from the homogeneous material regions would be representative of the complex simulation.

This paper presents an exploration that was setup to walk through defined parameter spaces to find the ionization, temperature, and density that best fit the forward and backward scattering spectra individually. The parameter space assumed a uniform distribution with linear sampling for the electron temperature,  $1 \leq T_e(\text{eV}) \leq 10^3$ , and ionization,  $0 \leq Z \leq 1$ , while taking a logarithmic sampling for the electron density,  $10^{20} \leq n_e(\text{cm}^{-3}) \leq 5 \times 10^{24}$ . A large sampling space was used, so no bias was placed on the resultant parameters.

The MCMC code works by calculating the likelihood of finding a specific set of parameters,  $\Theta$ , given the synthetic experimental spectrum,  $I_{\text{raw}}$ , at each step using Bayesian inference,

$$P(\Theta|I_{\text{raw}}) = \frac{P(I_{\text{raw}}|\Theta)P(\Theta)}{P(I_{\text{raw}})}, \quad (5)$$

where  $P(\Theta)$  is the prior distribution of possible parameters,  $P(I_{\text{raw}})$  is the marginal likelihood of the observed data over all possible parameters, and  $P(I_{\text{raw}}|\Theta)$  is the likelihood of finding  $I_{\text{raw}}$  given the input parameters,  $\Theta$ . The forward model likelihood,  $P(I_{\text{raw}}|\Theta) = e^{-\beta_{\text{cost}}}$ , is a user defined function that gives an acceptance percentage for each  $\Theta$ ,



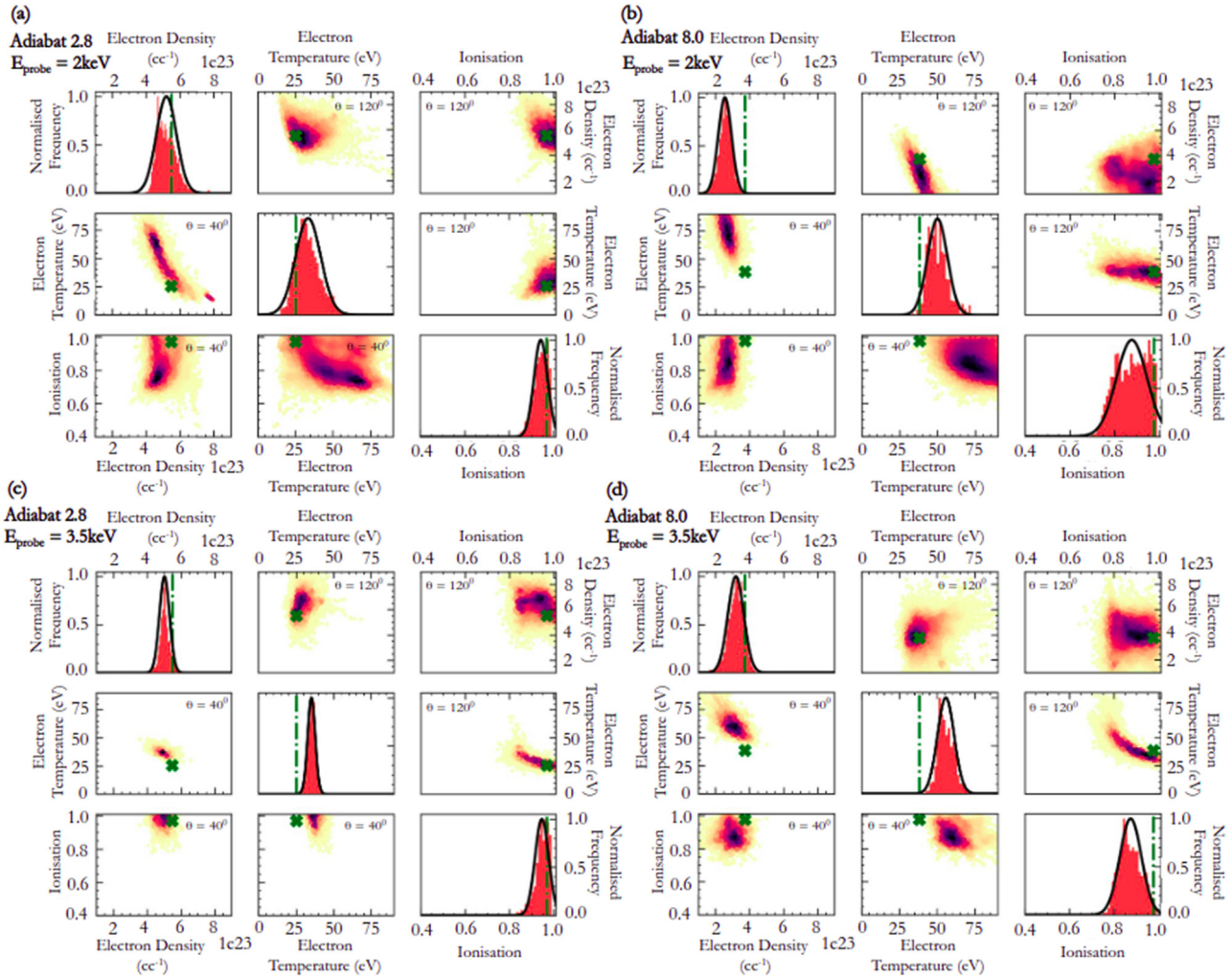


**FIG. 8.** MCMC parameter convergence fitting the entire spectrum using Eq. (6) as a cost function. Variation in DT plasma parameters from (a) 2.8 adiabat and 2 keV probe, (b) 8.0 adiabat and 2 keV probe, (c) 2.8 adiabat and 3.5 keV probe, and (d) 8.0 adiabat and 3.5 keV probe. The scatter plots show the correlation between each DT parameter. The lower quadrant scatter plots are taken from the 40° scattering data, while the upper quadrant shows the 120° scattering data. The scatter plots have been colored to represent the spatial density of points. The diagonal plots show the combined histograms for each parameter from both the scattering regimes. Superimposed on each histogram is a normal distribution of the fits. The mass-averaged parameter values from the LILAC 1D simulation are highlighted as a green dashed line or cross.

**TABLE I.** The full spectral analysis MCMC DT fitting parameters, as shown in Figs. 7 and 8, compared to the mass-weighted parameters from the LILAC 1D simulations, focused on the compressed DT shell, for each adiabat and each probe.

DT parameter	$T_e$ (eV)	$n_e$ ( $\text{cm}^{-3}$ )	Z
Adiabat 2.8			
Simulation	25	$5.5 \times 10^{23}$	0.97
MCMC 2 keV	$33 \pm 8$	$(5.2 \pm 0.6) \times 10^{23}$	$0.94 \pm 0.03$
MCMC 3.5 keV	$25 \pm 3$	$(5.0 \pm 0.3) \times 10^{23}$	$0.95 \pm 0.03$
Adiabat 8.0			
Simulation	38	$3.7 \times 10^{23}$	0.97
MCMC 2 keV	$50 \pm 6$	$(2.6 \pm 0.4) \times 10^{23}$	$0.88 \pm 0.07$
MCMC 3.5 keV	$56 \pm 6$	$(3.2 \pm 0.5) \times 10^{23}$	$0.87 \pm 0.05$

thus allowing convergence to be found on a parameter space that falls within the experimental noise.

The cost function used to determine the appropriateness of each MCMC spectra calculates the maximum percentage error, to allow equal weighting of the fitting to the elastic and inelastic peaks, between the MCMC spectrum,  $I_{\text{fit}}$ , and the synthetic experimental spectrum,  $I_{\text{raw}}$ ,

$$\beta_{\text{cost}} = \max \left( \frac{I_{\text{fit}} - I_{\text{raw}}}{I_{\text{raw}}} \frac{1}{\sqrt{2}\sigma} \right)^2, \quad (6)$$

where  $\sigma$  is the standard deviation representative of the noise of the synthetic scattering spectra. In an actual experiment, the value of  $\sigma$  is not known *a priori*, and it must be chosen for MCMC to be able to explore a sufficiently wide parameter space. For this analysis,  $\sigma = 0.075$ , which produces a range of accepted MCMC fits, as shown

in Fig. 7. The  $\sigma$  is selected, such that the noise of the scattering signal falls comfortably within the spread of the accepted fits. While using a cost function such as the sum of squares would produce an overall tighter fit to the spectra, this method assumes a perfect fitting model, which can lead to high confidence in false results.<sup>55</sup>

To analyze the MCMC data, the DT parameters were plotted on a combined matrix shown in Fig. 8. The scatter plots for each scattering angle are shown separately and have been colored to represent the spatial density of points. In Fig. 8, the histograms along the diagonal are the combined histograms for both the forward and backward scattering parameters. The mean and standard deviation on each parameter was calculated by fitting a normal distribution to the histograms.

The MCMC parameters were compared to the mass-weighted parameters from the 1D LILAC simulations. The mass-weighted simulation values were calculated as follows:

$$\langle F \rangle = \frac{\sum F_i \rho_i 4\pi r_i^2 dr_i}{\sum \rho_i 4\pi r_i^2 dr_i}, \quad (7)$$

where  $F_i$  is the desired parameter in zone  $i$ . The mass-weighted parameters were determined for each region of the implosion. It can be seen in Table I that the MCMC values are in close agreement with the mass-weighted parameters from the compressed DT shell. As discussed previously, this was an expected result, as the high density in the compressed shell meant that it dominated the inelastic scattering features.

## V. DISCUSSION

There is good agreement between the mass-averaged simulation parameter values and the MCMC distributions. This was the predicted result, as the high density and relative homogeneity of the compressed DT shell region dominate the spectrum. The forward scattering fits tend to converge around lower densities, higher temperatures, and broader ionizations. This results in either broader or slightly skewed distributions on the DT parameters. This differing numerical convergence occurs because the ratio between the source photon energy FWHM and the width of the inelastic scattering feature in the forward scattering case is very small, particularly for the 2 keV probe. It would, therefore, be possible to obtain information on the compressed DT conditions solely using a backward scattering detector. In particular, it should be noted that as can be seen from the parameter density maps in Fig. 8, analysis focusing solely on the backward scattering spectra would result in significantly better fits to the electron temperature. In order to improve the fit in the forward scattering regime, either a narrower bandwidth or a higher energy source should be used.

Information obtained regarding the CH plasma is predictably very little. This is due to its lower density compared to the DT compressed shell, meaning it does not contribute to the overall shape of the scattering feature as discussed previously. This, therefore, means that the weighting of the CH plasma in the MCMC analysis becomes very small, and convergence around representative conditions does not occur.

Overall, the optimum analysis presented in this paper to resolve the plasma conditions in the compressed shell, using a realistic laser probe from OMEGA EP, is performing MCMC analysis from spectra produced using a backward fielding detector. Using this methodology,

the overarching goal of resolving the high and low adiabat implosion conditions was achieved. As the collective forward scattering detector is not required for sufficient convergence on the DT compressed shell parameters, either a 2, 3.5 keV or higher energy x-ray photon energy probe could be used. Better agreement may be achieved between the MCMC parameters and the simulations if a narrower bandwidth (<10 eV) probe beam could be used, meaning that the forward scattering inelastic signal would be more sensitive to the electron density. In fact, this is what would be feasible with a free electron laser.<sup>57</sup>

In the future, similar analysis will be performed on the conditions at stagnation, the effect of mixing in the implosion, and investigations into 2D and 3D simulations using DRACO<sup>58</sup> and ASTER.<sup>59</sup> In addition, research and development on a spectrometer to optimize the detection of the XRTS signal is required to meet the constraints shown in this paper.

## VI. CONCLUSIONS

In summary, spatially integrated XRTS spectra for 1D LILAC simulated conditions of low- and high-adiabat, DT cryogenic implosions have been calculated at two-thirds convergence. Markov-chain Monte Carlo analysis was performed for two different scattering setups. Information on the compressed shell conditions was obtained as it has been shown to be possible to use the spectral resolution in a spatially integrated measurement to discriminate between different regions in the plasma. Fielding just one detector in the noncollective scattering regime produces good agreement with the compressed shell mass-averaged parameters from the simulation. This technique can be used to resolve both the low- and high-adiabat implosions.

## ACKNOWLEDGMENTS

This material is based upon work supported by the Department of Energy National Nuclear Security Administration under Award No. DE-NA0003856, the University of Rochester, and the New York State Energy Research and Development Authority.

This report was prepared as an account of work sponsored by an agency of the U.S. Government. Neither the U.S. Government nor any agency thereof, nor any of their employees, makes any warranty, express or implied, or assumes any legal liability or responsibility for the accuracy, completeness, or usefulness of any information, apparatus, product, or process disclosed, or represents that its use would not infringe privately owned rights. Reference herein to any specific commercial product, process, or service by trade name, trademark, manufacturer, or otherwise does not necessarily constitute or imply its endorsement, recommendation, or favoring by the U.S. Government or any agency thereof. The views and opinions of authors expressed herein do not necessarily state or reflect those of the U.S. Government or any agency thereof.

M.F.K. and S.M.V. acknowledge support from the UK EPSRC under Grant No. EP/P015794/1 and the Royal Society. S.M.V. is a Royal Society University Research Fellow.

The authors would also like to acknowledge the unnamed reviewer for providing insightful comments and suggestions to strengthen this manuscript.

## AUTHOR DECLARATIONS

## Conflict of Interest

The authors have no conflicts to disclose.

## Author Contributions

**H. Poole:** Conceptualization (equal); Data curation (lead); Formal analysis (lead); Investigation (lead); Methodology (lead); Writing – original draft (lead); Writing – review and editing (lead). **D. Cao:** Data curation (equal); Software (equal); Writing – review and editing (equal). **R. Epstein:** Methodology (supporting); Validation (supporting); Writing – review and editing (supporting). **I. Golovkin:** Resources (equal); Software (lead); Supervision (supporting); Validation (supporting). **T. Walton:** Investigation (equal); Software (equal); Writing – original draft (equal). **S. X. Hu:** Data curation (supporting); Software (supporting); Writing – review and editing (supporting). **M. Kasim:** Methodology (equal); Software (lead). **S. M. Vinko:** Funding acquisition (supporting); Methodology (supporting); Software (equal); Supervision (supporting); Writing – review and editing (equal). **J. R. Rygg:** Conceptualization (supporting); Investigation (supporting); Writing – review and editing (equal). **V. N. Goncharov:** Data curation (supporting). **G. Gregori:** Conceptualization (equal); Funding acquisition (equal); Investigation (supporting); Methodology (supporting); Resources (equal); Software (lead); Supervision (lead); Validation (equal); Writing – review and editing (equal). **S. P. Regan:** Conceptualization (equal); Funding acquisition (lead); Investigation (supporting); Methodology (supporting); Resources (equal); Supervision (lead); Writing – review and editing (equal).

## DATA AVAILABILITY

The data that support the findings of this study are available from the corresponding author upon reasonable request.

## REFERENCES

- <sup>1</sup>J. D. Lindl, P. Amendt, R. L. Berger, S. G. Glendinning, S. H. Glenzer, S. W. Haan, R. L. Kauffman, O. L. Landen, and L. J. Suter, *Phys. Plasmas* **11**, 339 (2004).
- <sup>2</sup>O. A. Hurricane, D. A. Callahan, D. T. Casey, P. M. Celliers, C. Cerjan, E. L. Dewald, T. R. Dittrich, T. Döppner, D. E. Hinkel, L. F. B. Hopkins, J. L. Kline, S. L. Pape, T. Ma, A. G. MacPhee, J. L. Milovich, A. Pak, H.-S. Park, P. K. Patel, B. A. Remington, J. D. Salmonson, and P. T. S. R. Tommasini, *Nature* **506**, 343 (2014).
- <sup>3</sup>S. P. Regan, V. N. Goncharov, T. C. Sangster, E. M. Campbell, R. Betti, J. W. Bates, K. Bauer, T. Bernat, S. Bhandarkar, T. R. Boehly, M. J. Bonino, A. Bose, D. Cao, L. Carlson, R. Chapman, T. Chapman, G. W. Collins, T. J. B. Collins, R. S. Craxton, J. A. Delettrez, D. H. Edgell, R. Epstein, M. Farrell, C. J. Forrest, R. K. Follett, J. A. Frenje, D. H. Froula, M. G. Johnson, C. R. Gibson, L. Gonzalez, C. Goyon, V. Y. Glebov, V. Gopalaswamy, A. Greenwood, D. R. Harding, M. Hohenberger, S. X. Hu, H. Huang, J. Hund, I. V. Igumenshchev, D. W. Jacobs-Perkins, R. T. Janezic, M. Karasik, J. H. Kelly, T. J. Kessler, J. P. Knauer, T. Z. Kosc, R. Luo, S. J. Loucks, J. A. Marozas, F. J. Marshall, M. Mauldin, R. L. McCrory, P. W. McKenty, D. T. Michel, P. Michel, J. D. Moody, J. F. Myatt, A. Nikroo, P. M. Nilson, S. P. Obenschain, J. P. Palastro, J. Peebles, R. D. Petrasso, N. Petta, P. B. Radha, J. E. Ralph, M. J. Rosenberg, S. Sampat, A. J. Schmitt, M. J. Schmitt, M. Schoff, W. Seka, R. Shah, J. R. Rygg, J. G. Shaw, R. Short, W. T. Shmayda, M. J. Shoup, A. Shvydky, A. A. Solodov, C. Sorce, M. Stadermann, C. Stoeckl, W. Sweet, C. Taylor, R. Taylor, W. Theobald, D. P. Turnbull, J. Ulreich, M. D. Wittman, K. M. Woo, K. Youngblood, and J. D. Zuegel, *Nucl. Fusion* **59**(3), 032007 (2018).
- <sup>4</sup>V. N. Goncharov, S. P. Regan, E. M. Campbell, T. C. Sangster, P. B. Radha, J. F. Myatt, D. H. Froula, R. Betti, T. R. Boehly, J. A. Delettrez, D. H. Edgell, R. Epstein, C. J. Forrest, V. Y. Glebov, D. R. Harding, S. X. Hu, I. V. Igumenshchev, F. J. Marshall, R. L. McCrory, D. T. Michel, W. Seka, A. Shvydky, C. Stoeckl, W. Theobald, and M. Gatu-Johnson, *Nucl. Fusion* **59**, 014008 (2017).
- <sup>5</sup>E. M. Campbell, V. N. Goncharov, T. C. Sangster, S. P. Regan, P. B. Radha, R. Betti, J. F. Myatt, D. H. Froula, M. J. Rosenberg, I. V. Igumenshchev, W. Seka, A. A. Solodov, A. V. Maximov, J. A. Marozas, T. J. B. Collins, D. Turnbull, F. J. Marshall, A. Shvydky, J. P. Knauer, R. L. McCrory, A. B. Sefkow, M. Hohenberger, P. A. Michel, T. Chapman, L. Masse, C. Goyon, S. Ross, J. W. Bates, M. Karasik, J. Oh, J. Weaver, A. J. Schmitt, K. Obenschain, S. P. Obenschain, S. Reyes, and B. V. Wouterghem, *Nucl. Fusion* **2**, 37 (2017).
- <sup>6</sup>J. A. Gaffney, S. X. Hu, P. Arnault, A. Becker, L. X. Benedict, T. R. Boehly, P. M. Celliers, D. M. Ceperley, O. Čertík, J. Clérouin, G. W. Collins, L. A. Collins, J.-F. Danel, N. Desbiens, M. W. C. Dharma-wardana, Y. H. Ding, A. Fernandez-Panella, M. C. Gregor, P. E. Grabowski, S. Hamel, S. B. Hansen, L. Harbour, X. T. He, D. D. Johnson, W. Kang, V. V. Karasiev, L. Kazandjian, M. D. Knudson, T. Ogitsu, C. Pierleoni, R. Piron, R. Redmer, G. Robert, D. Saumon, A. Shamp, T. Sjöstrom, A. V. Smirnov, C. E. Starrett, P. A. Sterne, A. Wardlow, H. D. Whitley, B. Wilson, P. Zhang, and E. Zurek, *High Energy Density Phys.* **28**, 7 (2018).
- <sup>7</sup>S. X. Hu, B. Militzer, V. N. Goncharov, and S. Skupsky, *Phys. Rev. Lett.* **104**, 235003 (2010).
- <sup>8</sup>S. X. Hu, L. A. Collins, T. R. Boehly, Y. H. Ding, P. B. Radha, V. N. Goncharov, V. V. Karasiev, G. W. Collins, S. P. Regan, and E. M. Campbell, *Phys. Plasmas* **25**, 056306 (2018).
- <sup>9</sup>S. X. Hu, *Phys. Rev. Lett.* **119**, 065001 (2017).
- <sup>10</sup>C. Wang, Y. Long, X. He, J.-F. Wu, W.-H. Ye, and P. Zhang, *Phys. Rev. E* **88**, 013106 (2013).
- <sup>11</sup>S. M. Vinko, O. Ciricosta, and J. S. Wark, *Nat. Commun.* **5**, 3533 (2014).
- <sup>12</sup>D. A. Chapman, J. Vorberger, L. B. Fletcher, R. A. Baggott, L. Divol, T. Döppner, R. W. Falcone, S. H. Glenzer, G. Gregori, T. M. Guymier, A. L. Kritcher, O. L. Landen, T. Ma, A. E. Pak, and D. O. Gericke, *Nat. Commun.* **6**, 6839 (2015).
- <sup>13</sup>T. G. White, N. J. Hartley, B. Borm, B. J. B. Crowley, J. W. O. Harris, D. C. Hochhaus, T. Kaempfer, K. Li, P. Neumayer, L. K. Pattison, F. Pfeifer, S. Richardson, A. P. L. Robinson, I. Uschmann, and G. Gregori, *Phys. Rev. Lett.* **112**, 145005 (2014).
- <sup>14</sup>P. Grabowski, S. Hansen, M. Murillo, L. Stanton, F. Graziani, A. Zylstra, S. Baalrud, P. Arnault, A. Baczewski, L. Benedict, C. Blancard, O. Čertík, J. Clérouin, L. Collins, S. Copeland, A. Correa, J. Dai, J. Daligault, M. Desjarlais, M. Dharma-wardana, G. Faussurier, J. Haack, T. Haxhimali, A. Hayes-Sterbenz, Y. Hou, S. Hu, D. Jensen, G. Jungman, G. Kagan, D. Kang, J. Kress, Q. Ma, M. Marcianti, E. Meyer, R. Rudd, D. Saumon, L. Shulenburg, R. Singleton, T. Sjöstrom, L. Stanek, C. Starrett, C. Ticknor, S. Valaitis, J. Venzke, and A. White, *High Energy Density Phys.* **37**, 100905 (2020).
- <sup>15</sup>O. A. Hurricane, P. T. Springer, P. K. Patel, D. A. Callahan, K. Baker, D. T. Casey, L. Divo, T. Döppner, D. E. Hinkel, M. Hohenberger, L. F. B. Hopkins, C. Jarrott, A. Kritcher, S. L. Pape, S. Maclaren, L. Masse, A. Pak, J. Ralph, C. Thomas, P. Volegov, and A. Zylstra, *Phys. Plasmas* **26**, 052704 (2019).
- <sup>16</sup>V. Y. Glebov, T. C. Sangster, C. Stoeckl, J. P. Knauer, W. Theobald, K. L. Marshall, M. J. Shoup III, T. Buczek, M. Cruz, T. Duffy, M. Romanofsky, M. Fox, A. Pruney, M. J. Moran, R. A. Lerche, J. McNaney, J. D. Kilkenny, M. J. Eckart, D. Schneider, D. Munro, W. Stoeffl, R. Zacharias, J. J. Haslam, T. Clancy, M. Yeoman, D. Warwas, C. J. Horsfield, J.-L. Bourgade, O. Landoas, L. Disdier, G. A. Chandler, and R. J. Leeper, *Rev. Sci. Instrum.* **81**, 10D325 (2010).
- <sup>17</sup>S. P. Regan, K. Falk, G. Gregori, P. B. Radha, S. X. Hu, T. R. Boehly, B. J. B. Crowley, S. H. Glenzer, O. L. Landen, D. O. Gericke, T. Döppner, D. D. Meyerhofer, C. D. Murphy, T. C. Sangster, and J. Vorberger, *Phys. Rev. Lett.* **109**, 265003 (2012).
- <sup>18</sup>S. H. Glenzer and R. Redmer, *Rev. Mod. Phys.* **81**, 1625 (2009).
- <sup>19</sup>G. Gregori, S. H. Glenzer, K. B. Fournier, K. M. Campbell, E. L. Dewald, O. S. Jones, J. H. Hammer, S. B. Hansen, R. J. Wallace, and O. L. Landen, *Phys. Rev. Lett.* **101**, 045003 (2008).
- <sup>20</sup>D. A. Chapman, D. Kraus, A. L. Kritcher, B. Bachmann, G. W. Collins, R. W. Falcone, J. A. Gaffney, D. O. Gericke, S. H. Glenzer, T. M. Guymier, J. A. Hawreliak, O. L. Landen, S. L. Pape, T. Ma, P. Neumayer, J. Nilsen, A. Pak, R.



- Redmer, D. C. Swift, J. Vorberger, and T. Döppner, *Phys. Plasmas* **21**, 082709 (2014).
- <sup>21</sup>E. J. Gamboa, P. A. Keiter, R. P. Drake, K. Falk, D. S. Montgomery, and J. F. Benage, *High Energy Density Phys.* **11**, 75 (2014).
- <sup>22</sup>T. R. Boehly, D. L. Brown, R. S. Craxton, R. L. Keck, J. P. Knauer, J. H. Kelly, T. J. Kessler, S. A. Kumpan, S. J. Loucks, S. A. Letzring, F. J. Marshall, R. L. McCrory, S. F. B. Morse, W. Seka, J. M. Soures, and C. P. Verdon, *Opt. Commun.* **133**, 495 (1997).
- <sup>23</sup>E. J. Gamboa, C. M. Huntington, M. R. Trantham, P. A. Keiter, R. P. Drake, D. S. Montgomery, J. F. Benage, and S. A. Letzring, *Rev. Sci. Instrum.* **83**, 10E108 (2012).
- <sup>24</sup>P. Davis, T. Döppner, J. R. Rygg, C. Fortmann, L. Divol, A. Pak, L. Fletcher, A. Becker, B. Holst, P. Sperling, R. Redmer, M. P. Desjarlais, P. Celliers, G. W. Collins, O. L. Landen, R. W. Falcone, and S. H. Glenzer, *Nat. Commun.* **7**, 11189 (2016).
- <sup>25</sup>A. K. Kritcher, T. Döppner, C. Fortmann, T. Ma, O. L. Landen, R. Wallace, and S. H. Glenzer, *Phys. Rev. Lett.* **107**, 015002 (2011).
- <sup>26</sup>L. B. Fletcher, A. L. Kritcher, A. Pak, T. Ma, T. Döppner, C. Fortmann, L. Divol, O. S. Jones, O. L. Landen, H. A. Scott, J. Vorberger, D. A. Chapman, D. O. Gericke, B. A. Mattern, G. T. Seidler, and G. Gregori, *Phys. Rev. Lett.* **112**, 145004 (2014).
- <sup>27</sup>J. Lindl, *Inertial Confinement Fusion* (Springer, New York, 1998).
- <sup>28</sup>R. S. Craxton, K. S. Anderson, T. R. Boehly, V. N. Goncharov, D. R. Harding, J. P. Knauer, R. L. McCrory, P. W. McKenty, D. D. Meyerhofer, J. F. Myatt, A. J. Schmitt, J. D. Sethian, R. W. Short, S. Skupsky, W. Theobald, W. L. Kruer, K. Tanaka, R. Betti, T. J. B. Collins, J. A. Delettrez, S. X. Hu, J. A. Marozas, A. V. Maximov, D. T. Michel, P. B. Radha, S. P. Regan, T. C. Sangster, W. Seka, A. A. Solodov, J. M. Soures, C. Stoeckl, and J. D. Zuegel, *Phys. Plasmas* **22**, 110501 (2015).
- <sup>29</sup>R. Betti and O. Hurricane, *Nat. Phys.* **12**, 435 (2016).
- <sup>30</sup>S. Atzeni and J. Meyer-Ter-Vehn, *The Physics of Inertial Fusion* (Oxford University Press, 2004).
- <sup>31</sup>O. L. Landen, D. T. Casey, J. M. DiNicola, T. Döppner, E. P. Hartouni, D. E. Hinkel, L. F. B. Hopkins, M. Hohenberger, A. L. Kritcher, S. L. Pape, B. J. MacGowan, S. Maclaren, K. D. Meaney, M. Millot, P. K. Patel, J. Park, L. A. Pickworth, H. F. Robey, J. S. Ross, S. T. Yang, A. B. Zylstra, K. L. Baker, D. A. Callahan, P. M. Celliers, M. J. Edwards, O. A. Hurricane, J. D. Lindl, J. D. Moody, J. Ralph, V. A. Smalyuk, C. A. Thomas, B. M. V. Wonerghem, and C. R. Weber, *High Energy Density Phys.* **36**, 100755 (2020).
- <sup>32</sup>M. J. Edwards, P. K. Patel, J. D. Lindl, L. J. Atherton, S. H. Glenzer, S. W. Haan, J. D. Kilkenny, O. L. Landen, E. I. Moses, A. Nikroo, R. Petrasso, T. C. Sangster, P. T. Springer, S. Batha, R. Benedetti, L. Bernstein, R. Betti, D. L. Bleuel, T. R. Boehly, D. K. Bradley, J. A. Caggiano, D. A. Callahan, P. M. Celliers, C. J. Cerjan, K. C. Chen, D. S. Clark, G. W. Collins, E. L. Dewald, L. Divol, S. Dixit, T. Döppner, D. H. Edgell, J. E. Fair, M. Farrell, R. J. Fortner, J. Frenje, M. G. G. Johnson, E. Giraldez, V. Y. Glebov, G. Grim, B. A. Hammel, A. V. Hamza, D. R. Harding, S. P. Hatchett, N. Hein, H. W. Herrmann, D. Hicks, D. E. Hinkel, M. Hoppe, W. W. Hsing, N. Izumi, B. Jacoby, O. S. Jones, D. Kalantar, R. Kauffman, J. L. Kline, J. P. Knauer, J. A. Koch, B. J. Koziolowski, G. Kyrala, K. N. LaFortune, S. L. Pape, R. J. Leeper, R. Lerche, T. Ma, B. J. MacGowan, A. J. MacKinnon, A. MacPhee, E. R. Mapoles, M. M. Marinak, M. Mauldin, P. W. McKenty, M. Meezan, P. A. Michel, J. Milovich, J. D. Moody, M. Moran, D. H. Munro, C. L. Olson, K. Opachich, A. E. Pak, T. Parham, H.-S. Park, J. E. Ralph, S. P. Regan, B. Remington, H. Rinderknecht, H. F. Robey, M. Rosen, S. Ross, J. D. Salmonson, J. Sater, D. H. Schneider, F. H. Séguin, S. M. Sepke, D. A. Shaughnessy, V. A. Smalyuk, B. K. Spears, C. Stoeckl, W. Stoeffl, L. Suter, C. A. Thomas, R. Tommasini, R. P. Town, S. V. Weber, P. J. Wegner, K. Widman, M. Wilke, D. C. Wilson, C. B. Yeamans, and A. Zylstra, *Phys. Plasmas* **20**, 070501 (2013).
- <sup>33</sup>K. Anderson and R. Betti, *Phys. Plasmas* **11**, 5 (2004).
- <sup>34</sup>J. Melvin, H. Lim, V. Rana, B. Cheng, J. Glimm, D. H. Sharp, and D. C. Wilson, *Phys. Plasmas* **22**, 022708 (2015).
- <sup>35</sup>T. R. Dittrich, O. A. Hurricane, D. A. Callahan, E. L. Dewald, T. Döppner, D. E. Hinkel, L. F. B. Hopkins, S. L. Pape, T. Ma, J. L. Milovich, J. C. Moreno, P. K. Patel, H.-S. Park, B. A. Remington, J. D. Salmonson, and J. L. Kline, *Phys. Rev. Lett.* **112**, 055002 (2014).
- <sup>36</sup>C. Cerjan, P. T. Springer, and S. M. Sepke, *Phys. Plasmas* **20**, 056319 (2013).
- <sup>37</sup>V. Gopalaswamy, R. Betti, J. P. Knauer, N. Luciani, D. Patel, K. M. Woo, A. Bose, I. V. Igumenshchev, E. M. Campbell, K. S. Anderson, K. A. Bauer, M. J. Bonino, D. Cao, A. R. Christopherson, G. W. Collins, T. J. B. Collins, J. R. Davies, J. A. Delettrez, D. H. Edgell, R. Epstein, C. J. Forrest, D. H. Froula, V. Y. Glebov, V. N. Goncharov, D. R. Harding, S. X. Hu, D. W. Jacobs-Perkins, R. T. Janezic, J. H. Kelly, O. M. Mannion, A. Maximov, F. J. Marshall, D. T. Michel, S. Miller, S. F. B. Morse, J. Palastro, J. Peebles, P. B. Radha, S. P. Regan, S. Sampat, T. C. Sangster, A. B. Sefkow, W. Seka, R. C. Shah, W. T. Shmyada, A. Shvydlyk, C. Stoeckl, A. A. Solodov, W. Theobald, J. D. Zuegel, M. G. Johnson, R. D. Petrasso, C. K. Li, and J. A. Frenje, *Nature* **565**, 581 (2019).
- <sup>38</sup>V. N. Goncharov, T. C. Sangster, R. Betti, T. R. Boehly, M. J. Bonino, T. J. B. Collins, R. S. Craxton, J. A. Delettrez, D. H. Edgell, R. Epstein, R. K. Follett, C. J. Forrest, D. H. Froula, V. Y. Glebov, D. R. Harding, R. J. Henchen, S. X. Hu, I. V. Igumenshchev, R. Janezic, J. H. Kelly, T. J. Kessler, T. Z. Kosc, S. J. Loucks, J. A. Marozas, F. J. Marshall, A. V. Maximov, R. L. McCrory, P. W. McKenty, D. D. Meyerhofer, D. T. Michel, J. F. Myatt, R. Nora, P. B. Radha, S. P. Regan, W. Seka, W. T. Shmyada, R. W. Short, A. Shvydlyk, S. Skupsky, C. Stoeckl, B. Yaakobi, J. A. Frenje, M. Gatu-Johnson, R. D. Petrasso, and D. T. Casey, *Phys. Plasmas* **21**, 056315 (2014).
- <sup>39</sup>J. MacFarlane, I. Golovkin, P. Wang, P. R. Woodruff, and N. A. Pereyra, *High Energy Density Phys.* **3**, 181 (2007).
- <sup>40</sup>I. Golovkin, J. J. MacFarlane, P. Woodruff, I. Hall, G. Gregori, J. Bailey, E. Harding, T. Ao, and S. Glenzer, *High Energy Density Phys.* **9**, 510 (2013).
- <sup>41</sup>J. Delettrez, R. Epstein, M. Richardson, P. A. Jaanimagi, and B. L. Henke, *Phys. Rev. A* **36**, 3926 (1987).
- <sup>42</sup>C. Stoeckl, M. Bonino, C. Mileham, S. Regan, W. Theobald, T. Ebert, and S. Sander, *High Energy Density Phys.* **41**, 100973 (2021).
- <sup>43</sup>C. Stoeckl, M. Bedzyk, G. Brent, R. Epstein, G. Fiksel, D. Guy, V. N. Goncharov, S. X. Hu, S. Ingraham, D. W. Jacobs-Perkins, R. K. Jungquist, F. J. Marshall, C. Mileham, P. M. Nilson, T. C. Sangster, M. J. Shoup, and W. Theobald, *Rev. Sci. Instrum.* **85**, 11E501 (2014).
- <sup>44</sup>C. Stoeckl, R. Epstein, R. Betti, W. Bittle, J. A. Delettrez, C. J. Forrest, V. Y. Glebov, V. N. Goncharov, D. R. Harding, I. V. Igumenshchev, D. W. Jacobs-Perkins, R. T. Janezic, J. H. Kelly, T. Z. Kosc, R. L. McCrory, D. T. Michel, C. B. Mileham, P. W. McKenty, F. J. Marshall, S. F. B. Morse, S. P. Regan, P. B. Radha, B. Rice, T. C. Sangster, M. J. Shoup, W. T. Shmyada, C. Sorce, W. Theobald, J. Ulreich, M. D. Wittman, D. D. Meyerhofer, J. A. Frenje, M. G. Johnson, and R. D. Petrasso, *Phys. Plasmas* **24**, 056304 (2017).
- <sup>45</sup>M. K. Urry, G. Gregori, O. L. Landen, A. Pak, and S. H. Glenzer, *J. Quant. Spectrosc. Radiat. Transfer* **99**, 636 (2006).
- <sup>46</sup>I. V. Igumenshchev, D. H. Edgell, V. N. Goncharov, J. A. Delettrez, A. V. Maximov, J. F. Myatt, W. Seka, A. Shvydlyk, S. Skupsky, and C. Stoeckl, *Phys. Plasmas* **17**, 122708 (2010).
- <sup>47</sup>V. N. Goncharov, O. V. Gotchev, E. Vianello, T. R. Boehly, J. P. Knauer, P. W. McKenty, P. B. Radha, S. P. Regan, T. C. Sangster, S. Skupsky, V. A. Smalyuk, R. Betti, R. L. McCrory, D. D. Meyerhofer, and C. Chérifil-Clérrouin, *Phys. Plasmas* **13**, 012702 (2006).
- <sup>48</sup>S. X. Hu, B. Militzer, V. N. Goncharov, and S. Skupsky, *Phys. Rev. B* **84**, 224109 (2011).
- <sup>49</sup>S. X. Hu, L. A. Collins, V. N. Goncharov, J. D. Kress, R. L. McCrory, and S. Skupsky, *Phys. Rev. E* **92**, 043104 (2015).
- <sup>50</sup>S. X. Hu, L. A. Collins, V. N. Goncharov, T. R. Boehly, R. Epstein, R. L. McCrory, and S. Skupsky, *Phys. Rev. E* **90**, 033111 (2014).
- <sup>51</sup>G. Gregori, S. H. Glenzer, W. Rozmus, R. W. Lee, and O. L. Landen, *Phys. Rev. E* **67**, 026412 (2003).
- <sup>52</sup>B. J. B. Crowley and G. Gregori, *New J. Phys.* **15**, 015014 (2013).
- <sup>53</sup>H. Sawada, S. P. Regan, D. D. Meyerhofer, I. V. Igumenshchev, V. N. Goncharov, T. R. Boehly, R. Epstein, T. C. Sangster, V. A. Smalyuk, B. Yaakobi, G. Gregori, S. H. Glenzer, and O. L. Landen, *Phys. Plasmas* **14**, 122703 (2007).
- <sup>54</sup>A. M. Saunders, A. Jenei, T. Döppner, R. W. Falcone, D. Kraus, A. Kritcher, O. L. Landen, J. Nilsen, and D. Swift, *Rev. Sci. Instrum.* **87**, 11E724 (2016).
- <sup>55</sup>M. Kasim, T. P. Galligan, J. Topp-Muggleston, G. Gregori, and S. M. Vinko, *Phys. Plasmas* **26**, 112706 (2019).
- <sup>56</sup>C. Andrieu, N. de Freitas, A. Doucet, and M. Jordan, *Mach. Learn.* **50**, 5 (2003).
- <sup>57</sup>L. B. Fletcher, H. J. Lee, T. Döppner, E. Galtier, B. Nagler, P. Heimann, C. Fortmann, S. LePape, T. Ma, M. Millot, A. Pak, D. Turnbull, D. A. Chapman, D. O. Gericke, J. Vorberger, T. White, G. Gregori, M. Wei, B. Barbrel, R. W.



- Falcone, C.-C. Kao, H. Nuhn, J. Welch, U. Zastra, P. Neumayer, J. B. Hastings, and S. H. Glenzer, *Nat. Photonics* **9**, 274 (2015).
- <sup>58</sup>P. B. Radha, T. J. B. Collins, J. A. Delettrez, Y. Elbaz, R. Epstein, V. Y. Glebov, V. N. Goncharov, R. L. Keck, J. P. Knauer, J. A. Marozas, F. J. Marshall, R. L. McCrory, P. W. McKenty, D. D. Meyerhofer, S. P. Regan, T. C. Sangster, W. Seka, D. Shvarts, S. Skupsky, Y. Srebro, and C. Stoeckl, *Phys. Plasmas* **12**, 056307 (2005).
- <sup>59</sup>I. V. Igumenshchev, V. N. Goncharov, F. J. Marshall, J. P. Knauer, E. M. Campbell, C. J. Forrest, D. H. Froula, V. Y. Glebov, R. L. McCrory, S. P. Regan, T. C. Sangster, S. Skupsky, and C. Stoeckl, *Phys. Plasmas* **23**, 052702 (2016).